Acta Crystallographica Section D
Biological Crystallography
ISSN 0907-4449

Investigations of surrogate cellular membranes using neutron reflectometry

Manish Dubey,‡ Michael S. Jablin,‡ Hillary Smith and Jarosław Majewski*

Lujan Neutron Scattering Center, Los Alamos National Laboratory, Los Alamos, NM 87545, USA

‡ These authors contributed equally to this work.

Correspondence e-mail: jarek@lanl.gov

Received 10 April 2010
Accepted 13 May 2010

The nonperturbative nature of neutron reflectometry (NR) coupled with its isotopic sensitivity has made it an ideal candidate for the study of model biological membranes at the solid–liquid interface. In this article, methods are presented for the creation and characterization of supported model membranes which can mimic many of the critical attributes of cell membranes. It is demonstrated that NR can characterize the structure, composition and organization of model membranes deposited on solid, nanoporous and polymer supports. Additionally, *in situ* NR measurements of the interactions between model membranes and external stimuli are presented. Finally, an investigation of the adherence region of live mouse fibroblast cells is described.

1. Introduction

The plasma membrane encloses a cell, thereby defining its boundary and regulating its interaction with the external world. The biomembrane controls transport between the cell and its surroundings and therefore must be selectively permeable to specific molecules depending on the requirements of the enclosed cell (Alberts *et al.*, 2002). It follows that the wellbeing of a cell is critically related to the attributes of its plasma membrane, and therefore an understanding of the biomembrane structure and the effects of external stimuli on its behavior is important. Unfortunately, the complexity of plasma membranes makes physical and chemical characterization difficult, leading to the design of model systems which simplify cell membranes by only mimicking critical features of interest. Depending on the motive of a study and the tools used for investigation, a particular model membrane system (micelles, liposomes, monolayers at the air–water interface or supported bilayers at the solid–liquid interface) can be employed. Optical (Monzel *et al.*, 2009; Matsuzaki *et al.*, 2000), spectroscopic (Bindig *et al.*, 2000), microscopic (Goksu *et al.*, 2009), scattering (Harroun *et al.*, 2009) and a number of other techniques (Mozsolits & Aguilar, 2002; Gibbons *et al.*, 2006) have been utilized in the past to characterize biomembranes.

Neutron reflectometry (NR) is a tool which can probe biological structures in aqueous environments. Neutrons are scattered from nuclei and therefore their scattering intensity is a function of the nuclear constituents. This makes neutrons sensitive to different isotopes of the same element. For example, neutrons scatter weakly from water but strongly from heavy water (D_2O). Often, isotopic substitution allows scattering contrast variation without altering the biochemistry of the system, and it is particularly advantageous for investigations of biological samples because of the opportunity to modify the scattering intensity by exchanging deuterium for hydrogen. Since neutrons are weakly scattered by nuclei, they

can penetrate sample environments to probe buried interfaces and are often utilized to perform *in situ* characterization of biological systems in their natural aqueous environment, eliminating the possibility of denaturing (a major problem when using vacuum-based tools). Additionally, NR does not modify the structure of biological materials, unlike X-rays, because the neutrons typically used for NR do not cause significant beam damage to the sample.

We have used NR to study supported biomembranes and the effects of external stimuli on their structure. In addition to providing insight into biomembrane structure, these investigations have laid the foundation for the future use of supported membranes in bio-sensing applications. This article summarizes our efforts in (i) creating model biomembranes, (ii) investigating their structure on solid, polymer and nanoporous supports and (iii) understanding their interactions with external stimuli. While we have studied various model systems, our ultimate goal is to utilize our results to better understand the structure of cellular membranes. To this end, we have successfully used our model membrane experience to investigate the adhesion of live fibroblast cells to growth-medium-coated quartz substrates.

2. Deposition and sample environment

We have used two methods to create bilayers: vesicle fusion and Langmuir–Blodgett/Langmuir–Schaefer (LB/LS) deposition. To begin vesicle fusion, lipids are dissolved in a solvent, which is subsequently evaporated. Next, the lipids are rehydrated to form multilamellar vesicles (MVs), which unfortunately are stable and will not rupture to fuse over the surface of a substrate. MVs are therefore converted into small unilamellar vesicles (SUVs), which is commonly accomplished using sonication and extrusion, and the resulting SUVs rupture upon contact with a substrate to form a bilayer. To create a bilayer *via* vesicle fusion, the substrate should be hydrophilic and the lipids must be in the liquid phase.

LB/LS is a more controlled method than vesicle fusion for creating a lipid bilayer. Firstly, a lipid solution is spread onto the air–water interface in a Langmuir trough. Next, the monolayer is compressed while its surface pressure is monitored. To deposit the inner leaflet, a substrate is drawn through the air–water interface, coating the substrate face perpendicular to the water surface (LB). The monolayer surface pressure is maintained by consistent compression during the transfer. The substrate is then rotated so that its surface is parallel to the water surface and driven back through the air–water interface to deposit the outer leaflet (LS). Because the leaflets are deposited independently, membranes with the same (symmetric) and different (asymmetric) compositions in the inner and outer leaflets can be created. Additionally, the deposition surface pressure can be varied, which allows control of the phase of the membrane constituents.

All bilayers were measured in a solid–liquid interface cell (Fig. 1). The setup was composed of a substrate supported by an O-ring and a Macor ceramic disk (Ceramic Products Inc., Palisade Park, New Jersey, USA). The Macor, O-ring and substrate define a 0.2–0.3 mm thick reservoir for the subphase. The entire sample environment was held in place with aluminium clamps. Neutrons enter the lateral face of the substrate and are scattered from the substrate–subphase interface. D_2O provides neutron scattering contrast between the substrate, the hydrogen-rich bilayer and the subphase.

3. Neutron reflectometry

NR experiments were performed on the Surface Profile Analysis Reflectometer (SPEAR), a time-of-flight reflectometer at the Los Alamos National Laboratory Lujan Neutron Scattering Center. SPEAR receives neutrons from a polychromatic pulsed (20 Hz) source that pass through a partially coupled liquid-hydrogen moderator at 20 K to shift their energy spectrum. Choppers and frame-overlap mirrors reduce the wavelength range of the neutrons to 2–16 Å. The wavelength, λ, and the momentum of incident neutrons are related by the de Broglie relation, $\lambda = hp^{-1}$, where h is Planck's constant and p is the momentum of the neutron. By measuring the time it takes a neutron to travel the length of the instrument, the momentum and therefore the wavelength of the neutron can be determined. During an NR experiment, neutrons impinge on a sample at a small angle, θ, and the ratio of elastically scattered to incident neutrons is measured. This ratio is defined as the reflectivity, R, and is measured as a function of the momentum-transfer vector, Q_z, where $Q_z = 4\pi\sin(\theta)\lambda^{-1}$. The incident neutron beam is collimated with a series of slits to create a footprint on the sample of approximately 20 × 50 mm. The coherent area of the neutron beam projected onto the sample is approximately 1 × 100 µm and the acquired data are an average of the reflectivity from each coherent area that makes up the footprint. Because the average intensity over a large area is measured, the reflectivity is sensitive to the surface coverage of the membrane. The reflectometry data presented here are multiplied by Q_z^4 to

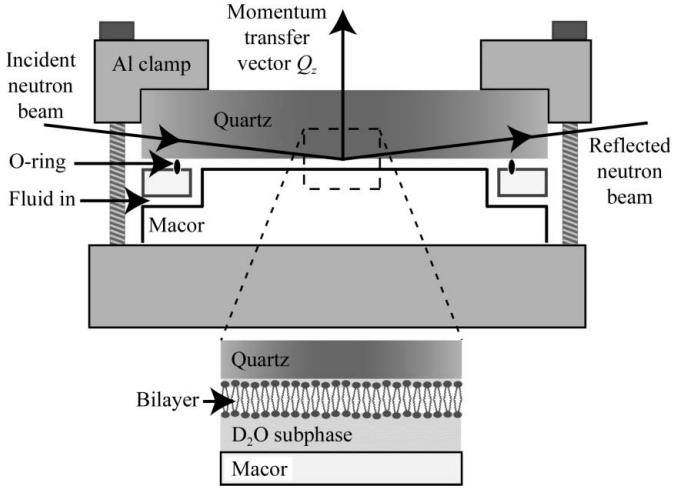

Figure 1
A schematic of the solid–liquid interface cell. After depositing a bilayer, the substrate is clamped against a Macor disk with a 0.2–0.3 mm thick subphase-filled gap created by an O-ring. The neutron beam penetrates the lateral face of the substrate and is scattered from the buried solid–liquid interface.

highlight deviations from the sharp decrease in reflectivity as described by Fresnel's law: $R \propto Q_z^{-4}$ (Als-Nielsen, 1986).

Analysis of specular reflectometry data provides information regarding the coherent scattering-length density (SLD) distribution normal to the surface of a sample, SLD(z), where z denotes the distance from the substrate. SLD is a value unique to a particular chemical composition and is the sum of the coherent scattering lengths of the constituent elements divided by the volume that they occupy. SLD values determined by NR are absolute because the data are normalized to the incident neutron intensity. To obtain a real-space interpretation of the scattering data, SLD(z), a Fourier transform can be applied. Because only intensity and no phase information is collected, a unique Fourier transform between a single NR profile and its real-space interpretation does not exist. Therefore, modeling was employed to interpret the NR data.

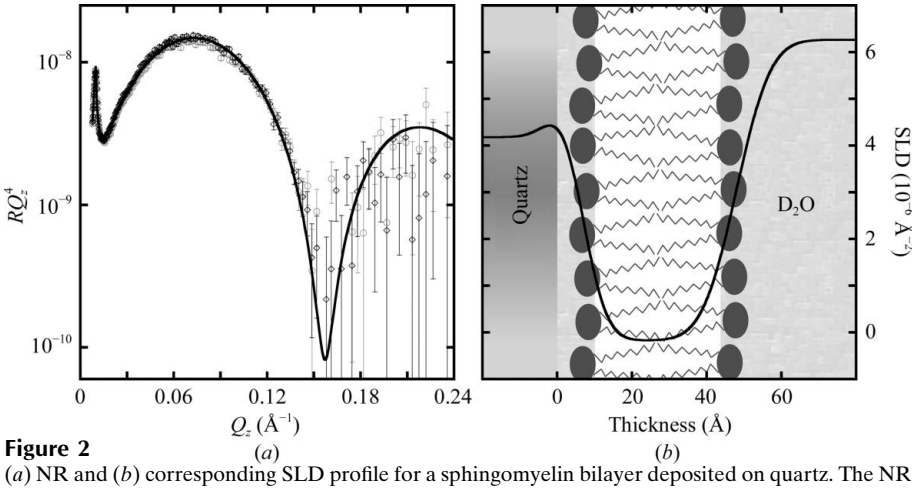

Figure 2
(*a*) NR and (*b*) corresponding SLD profile for a sphingomyelin bilayer deposited on quartz. The NR data are represented by open circles with error bars indicating one standard deviation. The black lines are the theoretical NR and SLD profiles. A real-space cartoon corresponding to the SLD profile also is depicted.

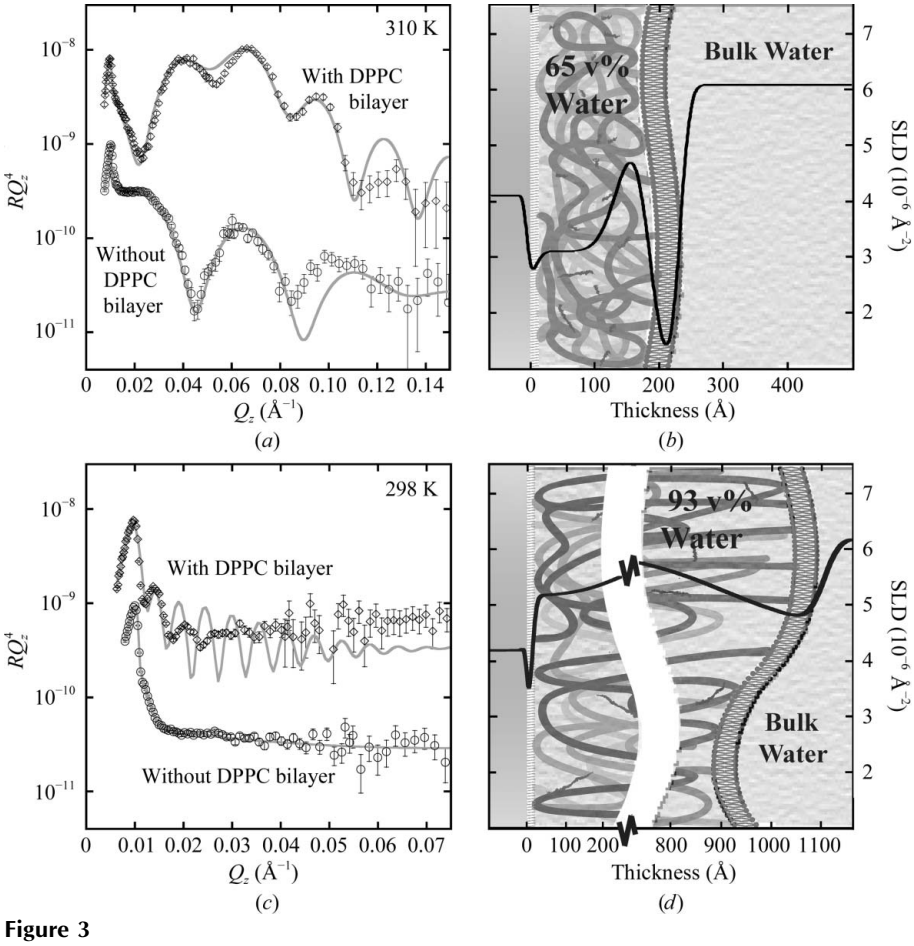

Figure 3
(*a*, *c*) NR and (*b*, *d*) corresponding SLD profiles for a polymer-supported lipid bilayer shown in collapsed and expanded states. The NR data are plotted using open shapes with error bars indicating one standard deviation. The solid lines are the best fits that correspond to the SLD profiles shown in (*b*) and (*d*).

The continuous function SLD(z) can often be well approximated by a number of layers, referred to as boxes, each with a constant SLD. Inter-layer roughness can be taken into account using an error function centered at each interface (Nevot & Croce, 1980). The incident neutron beam is refracted at each interface and a theoretical NR curve can be calculated using the Parratt recursion formula (Parratt, 1954). The measured and theoretical NR curves are compared and the best least-squares fit, corresponding to the lowest χ^2 value, is obtained using genetic optimization and the Levenburg–Marquardt nonlinear least-squares method (Nelson, 2006). The simplest SLD model (the least number of boxes) of physical relevance was used to understand the NR data.

4. Model biomembranes

It is accepted that supported lipid bilayers can be used to mimic cellular membranes (Chan & Boxer, 2007). However, many supported bilayer systems do not effectively model the deformability or natural curvature of cell membranes, which not only affects cellular adhesion processes but also alters the dynamics and localization of transmembrane proteins (Parthasarathy & Groves, 2007). Additionally, the development of nanostructured devices for sensing applications and their integration with biological systems has resulted in a demand for nano-supported bilayers. As described in this

section, our group has investigated several different support systems.

4.1. Solid supported bilayers

Silicon, quartz and mica are common substrates used to support bilayers at the solid–liquid interface (Benes *et al.*, 2004). Compared with monolayers at the air–water interface, which only represent a single biomembrane leaflet, the structure of supported bilayers is a better mimic of cellular membrane structure. Unfortunately, solid supported membranes must adopt a planar topography because of the proximity of the substrate, which also does not allow the incorporation of transmembrane proteins in their native configuration. Even though solid supported membranes lack in-plane and out-of-plane freedom compared with cellular membranes, they provide a system that facilitates investigation using various analytical tools. Using NR, many *in situ* structural membrane attributes (thickness, density, surface coverage and integrity) can be investigated.

We have used both vesicle fusion and LB/LS techniques to deposit lipid bilayers on quartz substrates. Fig. 2 shows NR data and the corresponding SLD profile for a sphingomyelin (SM; derived from chicken egg; Avanti Polar Lipids Inc., Alabaster, Alabama, USA) bilayer deposited at a surface pressure of 30 mN m^{-1} *via* LB/LS and characterized in a subphase of D_2O. The headgroups of the inner and outer leaflets are hydrated by D_2O and therefore scattering contrast is predominantly between the deuterated subphase and the hydrogenated lipid tails. The NR profile suggests a complete surface coverage and a thickness of 38 ± 2 Å (the theoretical value for two SM tails in contact is ~40 Å).

4.2. Polymer-supported bilayers

Two traditional types of supports for lipid bilayers include a thin lubricating layer of water or a hydrated polymer tether between the model membrane and the solid surface (Sackmann, 1996; McGillivray *et al.*, 2007). Although both of these supports are sufficient to maintain the lateral mobility of the constituent lipids, they constrain the lipid to a planar or nearly planar geometry. Cellular membranes possess a flexible three-dimensional dynamic structure. Therefore, an important goal for supported layers is to mimic the hydration and elasticity of the cellular matrix and to permit in-plane and out-of-plane undulations of the membrane. A flexible platform can facilitate the interaction between biomolecules and model membranes, thereby creating a more biologically relevant surrogate system.

We have demonstrated the use of a thermoresponsive polymer cushion to support a model membrane. The cushion can be collapsed in an aqueous environment to provide an ideal surface for membrane deposition and swollen to push the membrane off the surface and promote deviations from a planar geometry (Smith, Jablin *et al.*, 2009). The cushion is composed of poly(*N*-isopropylacrylamide) copolymerized with 3 mol% methacrylbenzophenone and cross-linked using ultraviolet light. At 310 K, a dipalmitoyl-*sn*-glycero-3-phosphocholine (DPPC; Avanti Polar Lipids Inc., Alabaster, Alabama, USA) membrane was deposited at a surface pressure of 40 mN m^{-1} *via* LB/LS onto a polymer-coated quartz substrate. Firstly, the supported membrane was characterized in D_2O when the underlying polymer was collapsed (310 K). The NR curve indicates the presence of a complete membrane which sits atop a 170 Å thick cushion (Fig. 3*a*). The corresponding SLD profiles with and without membrane are shown in Fig. 3(*b*). Next, the properties of the polymer-supported membrane were studied when the polymer was expanded (298 K). NR and corresponding SLD profiles for the polymer-supported membrane at 298 K are shown in Figs. 3(*c*) and 3(*d*), respectively. A polymer thickness of 900 Å (at 298 K; hydrated state) as opposed to 170 Å (at 310 K; collapsed state) is observed, which demonstrates the flexibility of the polymer cushion. Additionally, increased in-plane and out-of-plane membrane undulations were observed at 298 K, suggesting that once the underlying polymer cushion is swollen with water the membrane is free to adopt a more natural three-dimensional topography. By controlling the temperature, the thickness of the polymer cushion and thereby the distance between the supported membrane and the quartz substrate can be manipulated reversibly *in situ*.

4.3. Nanoporous-layer-supported bilayers

Advances in the understanding of material characteristics on the nanometer scale have resulted in widespread interest in studying the interaction of nanomaterials with biological systems. We have investigated various nanosystems (nanoporous silicon, carbon nanotubes *etc.*) as supports of model membranes which have applications in the field of biological sensors and disease diagnostics (Doshi *et al.*, 2005; Gagner *et al.*, 2006).

A nanocomposite film of silica was spin-coated onto a Si(111) substrate. We then used vesicle fusion to deposit SUVs of 1-palmitoyl-2-oleoyl-*sn*-glycero-3-phosphocholine (POPC; Avanti Polar Lipids Inc., Alabaster, Alabama, USA) onto the nanocomposite. The nanoporous supported bilayer was characterized in a deuterated subphase and Fig. 4 shows the NR and SLD profiles. The thickness of the underlying nanoporous support and the membrane can be extracted from the NR profile (the shorter and longer wavelength oscillations, respectively). The NR profile suggests a lipid-membrane thickness of approximately 35 Å. The lower than expected thickness is attributed to *gauche* defects or the tilting of the lipid tails. This experiment demonstrated that we could form continuous, uniform and stable bilayers of POPC on ordered nanocomposite and nanoporous silicon films (Doshi *et al.*, 2005).

5. Interaction with external stimuli

Biomembranes are necessarily complex because of the multitude of tasks that they perform. Many biological studies seek to understand not only biomembrane structure but also the structural changes induced upon interaction with external stimuli, which further increases the complexity and therefore

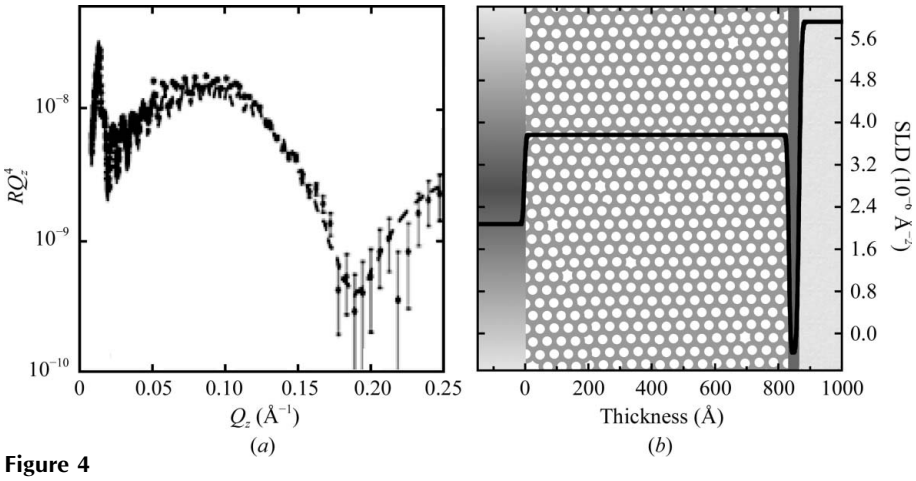

Figure 4
(*a*) NR curve and (*b*) corresponding SLD profile overlaid on a real-space depiction of POPC bilayers deposited on a silica nanoporous film. NR data are shown by closed circles with error bars that indicate one standard deviation. The solid lines are the best NR fit and correspond to the SLD profile. Short-wavelength oscillations in the NR profile arise from the 800 Å thick nanoporous layer. The long-wavelength oscillation arises from the thickness of the hydrogenated lipid membrane.

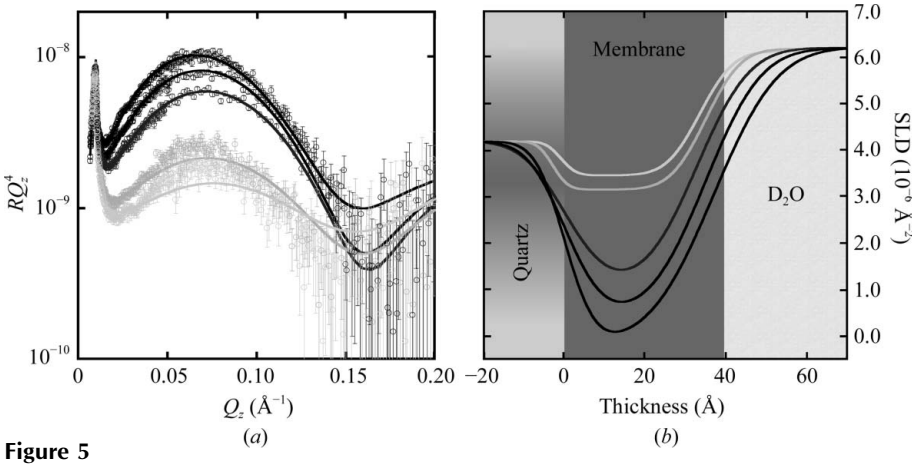

Figure 5
(*a*) NR and (*b*) corresponding SLD profiles of POPC bilayers upon incremental (15 min) exposure to UV light. In both plots, increased exposure time is shown in decreasing shades of gray. NR data are shown by open circles with error bars that indicate one standard deviation.

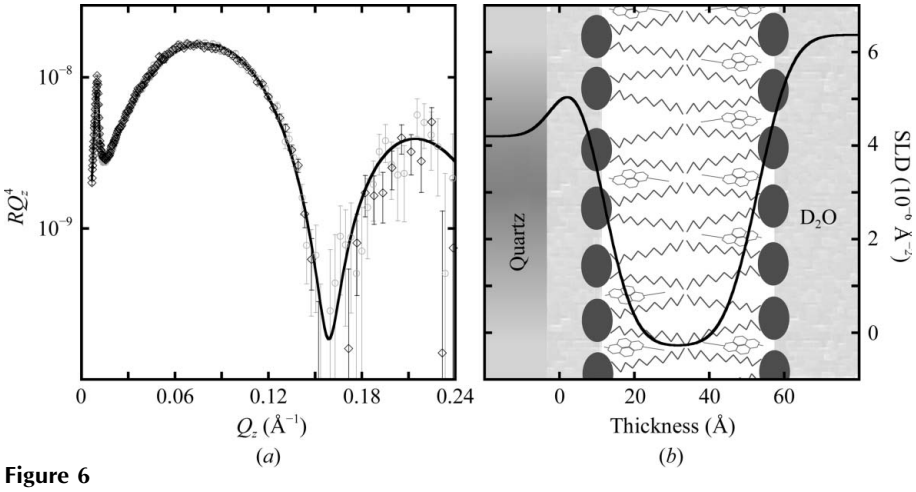

Figure 6
(*a*) NR and (*b*) corresponding SLD profiles for a 67:33 (SM:Chol) molar-ratio bilayer on quartz substrate. The measurements before (black diamonds) and after (gray circles) the introduction of the β-CD solution are shown, while the black line represents the fit and corresponding SLD profile. Error bars indicate one standard deviation. A real-space cartoon corresponding to the SLD profile is also depicted. The scattering from the system was unaffected by the introduction of β-CD.

the difficulty of the research. External stimuli can change the thickness, density, surface coverage and in-plane and out-of-plane topography of a biomembrane. Because NR is a nondestructive probe, it has been utilized for *in situ* investigations of the effects of oxidative stress and of the introduction of β-cyclodextrin on membrane structure.

5.1. Oxidative stress

Oxidation of biomembranes has been associated with a number of pathological conditions such as aging (Hsiai & Berliner, 2007), Alzheimer's disease (Markesbery & Carney, 1999) and apoptosis (Martinet & Kockx, 2001). Oxidation induces changes in the structure as well as in the physical and chemical properties of a membrane, thereby disrupting its ability to function (Megli & Russo, 2008). These structural modifications along with the subsequent reorganization of the membrane upon oxidative stress have been investigated *in situ* by NR. Bilayers composed of POPC were deposited using vesicle fusion in a subphase of D_2O and illuminated by ultraviolet (UV) light to induce oxidative stress. The structure of the membrane was determined as a function of UV exposure time. Fig. 5 shows NR data of a POPC bilayer exposed to UV light for 15 min increments up to a cumulative exposure of 60 min. The decrease in scattering intensity suggests structural changes in the membrane. We postulate that UV light generates reactive oxygen species which can break the double bonds found in the unsaturated tails of POPC, resulting in disruption of the bilayer. This disruption leads to the formation of pores in the membrane, which can subsequently be filled by the subphase. The incorporation of the deuterated (high SLD) subphase into the pores in the otherwise hydrogenated (low SLD) membrane results in an increased SLD value of the membrane layer. As the UV exposure time is increased, the membrane surface coverage decreases, resulting in a consistently increasing SLD value of the membrane layer (an increasing volume fraction of deuter-

ated subphase; Fig. 5*b*). In order to minimize the destruction of the membrane, L-ascorbic acid, a known antioxidant, was added to the subphase prior to UV exposure. POPC membranes in 0.1 *M* L-ascorbic acid solutions were completely unaffected by exposure to UV. Oxidative-stress studies were also conducted on DPPC and the results observed indicate a slower rate of decrease in coverage compared with POPC. DPPC is saturated and therefore less strongly affected by reactive oxygen species (Smith, Howland *et al.*, 2009).

5.2. Introduction of β-cyclodextrin

Ordered domains enriched in sphingolipids and cholesterol are referred to as lipid rafts and have unique physical and chemical properties compared with their disordered fluid surroundings (Simons & Ikonen, 1997). Lipid rafts are an integral part of cellular membranes and play a vital role in signal transduction and trafficking (Hanzal-Bayer & Hancock, 2007; Schutz *et al.*, 2000; Stauffer & Meyer, 1997) and sorting of lipids and proteins (Hanzal-Bayer & Hancock, 2007; McIntosh *et al.*, 2003; Schutz *et al.*, 2000; Stauffer & Meyer, 1997), as well as mitigating viral and bacterial infections (Slotte, 1999; Wang *et al.*, 2009). Lipid rafts are resistant to some molecules, such as β-cyclodextrin (β-CD), which are able to disturb less organized regions of a membrane. We used β-CD to probe the stability of model lipid rafts by *in situ* NR investigations. Model membranes consisting of varying molar ratios of sphingomyelin (SM) and cholesterol (Chol) above and below the accepted stable complexation ratio (67:33; Radhakrishnan & McConnell, 1999) were created *via* the LB/LS technique. The SM/Chol bilayers were characterized in D_2O by NR before and after introduction of β-CD to probe the influence of β-CD on the structure, composition and organization of the bilayers. The scattering from bilayers with proportions of Chol above the stable complexation ratio (no excess Chol) were unaffected by the introduction of β-CD. Fig. 6 shows representative NR and SLD profiles from a 67:33 molar-ratio membrane. These results suggest that β-CD is unable to remove Chol complexed with SM or pure SM. The structure of membranes below the stable complexation ratio (excess Chol) was dramatically modified by the introduction of β-CD (Fig. 7), suggesting that β-CD can remove all excess Chol beyond the stable complexation ratio. The removal of Chol is evident from the increased SLD value of the membrane layer (Fig. 7*b*) after the introduction of β-CD. As Chol is removed by β-CD, the membrane reorganizes to hide the exposed hydrophobic tails of the remaining SM and Chol from the subphase. Subsequently, D_2O is incorporated into the membrane layer (Jablin *et al.*, 2010).

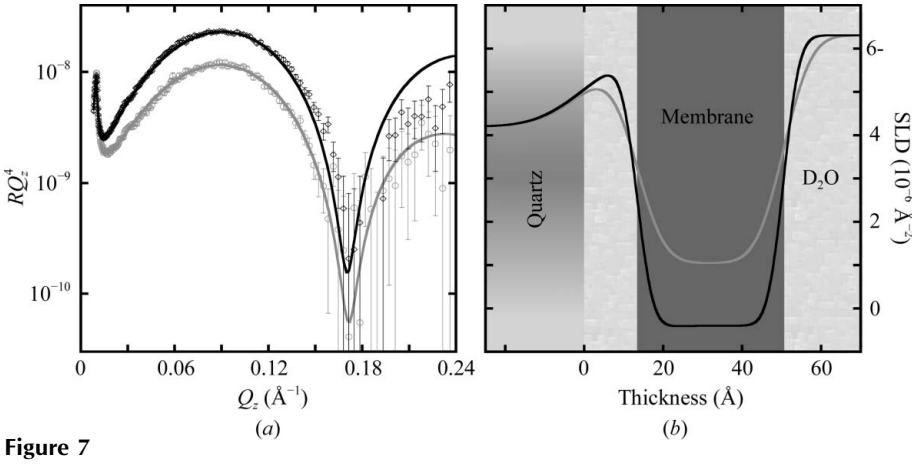

Figure 7
(*a*) NR and (*b*) corresponding SLD profile for a 33:67 (SM:Chol) molar-ratio bilayer on quartz substrate. The measurements before (black diamonds) and after (gray circles) the introduction of the β-CD solution are shown with error bars indicating one standard deviation. SLD profiles before and after introducing β-CD are shown by black and gray lines, respectively. A box diagram corresponding to the SLD profile is also depicted. The amplitude of the scattering decreases and the SLD of the membrane region increases, indicating the removal of all uncomplexed Chol, significant membrane reorganization and incorporation of D_2O into regions no longer occupied by membrane.

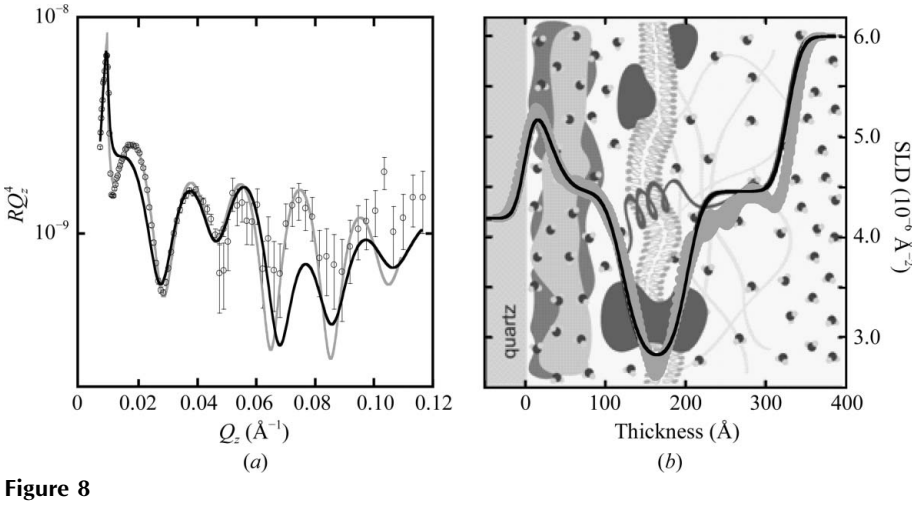

Figure 8
(*a*) NR and (*b*) corresponding SLD profile for fibroblast cells adhered to a growth-medium-coated quartz substrate. NR data are shown by open circles with error bars that indicate one standard deviation. The solid black and gray lines are the best NR fit and the corresponding SLD profile (model-dependent and model-independent, respectively). A real-space interpretation shows the structure of the cell-adherence region on the quartz surface. The layer closest to the substrate is composed of proteins produced by the cells on the growth media (~120 Å), the next layer represents the cell membrane closer to the substrate (~80 Å) and finally a diffuse transition to the SLD of deuterated PBS indicates the interior of the cell.

6. Cellular membranes

Investigations of model membranes can provide insight into many biomembrane attributes and have been utilized to decipher the complex structure–function relationship of cellular membranes in various environments. Some plasma-

membrane features cannot be replicated by model systems and a live cell must be studied. We have recently used our expertise in NR and model membranes to examine the adherence region of live mouse fibroblast cells on a media-coated quartz substrate in a deuterated PBS environment at room temperature. Fig. 8 shows the NR data and corresponding SLD profile for a high surface density of fibroblast cells. Both model-independent and model-dependent fitting procedures were employed (Pedersen & Hamley, 1994*a*,*b*). The result of model-independent fitting is a real-space interpretation of the NR data that is less biased by the experimenters' expectations of the SLD distribution. Iteratively running the model-independent fitting procedure and accepting all SLD profiles within χ of the best χ^2 profile produced a family of SLD profiles that are shown as a gray ribbon in Fig. 8(*b*). Model-dependent fitting was performed in an attempt to mimic this profile using the simplest possible box model. Both fitting methods provided very similar SLD profiles. The region of the cell closest to the substrate has a higher SLD, which is attributed to the proteins produced by the cells to adhere to the growth media. The decrease in the SLD in the region next to the adhered protein layer represents the membrane region. A steady increase in the SLD after the membrane region indicates the presence of deuterated PBS in the interior of the cell. A cartoon depiction of the cell membrane region is shown in Fig. 8(*b*) to facilitate interpretation of the SLD profile. We also have used NR to investigate the density of cell-surface coverage along with the effects of distilled water and trypsin (both of which are expected to disrupt the cells; Smith *et al.*, 2010).

7. Concluding remarks

NR has been demonstrated to be a powerful technique for the characterization of the structure of membranes at solid–liquid interfaces. Further advances in instrumentation promise to facilitate the study of complex systems such as living cells and model membranes with biopolymers and transmembrane proteins. Increased neutron flux and decreased background will allow an increased Q_z range to be measured, improving the out-of-plane resolution. Additionally, coupling an increase in flux with improved neutron optics will enable the creation of a smaller footprint on the sample (mm^2) without prohibitively increasing the experiment time, eliminating the current sample requirement of large-scale homogeneity (cm^2). Future two-dimensional detectors will allow the collection of the total scattering (specular, off-specular, grazing-incidence small angle and grazing-incidence diffraction) from a sample and subsequent analysis will provide both in-plane and out-of-plane (three-dimensional) structural information. Finally, improved sample chambers will allow experiments involving exotic environments.

This work benefited from the use of the Lujan Neutron Scattering Center at Los Alamos Neutron Science Center funded by the DOE Office of Basic Energy Sciences and Los Alamos National Laboratory under DOE Contract DE-AC52-06NA25396.

References

Alberts, B., Johnson, A., Lewis, J., Raff, M., Roberts, K. & Walter, P. (2002). *Molecular Biology of the Cell*, 4th ed. New York: Garland Science.
Als-Nielsen, J. (1986). *Physica A*, **140**, 376–389.
Benes, M., Billy, D., Benda, A., Speijer, H., Hof, M. & Hermens, W. T. (2004). *Langmuir*, **20**, 10129–10137.
Bindig, U., Meinke, M., Gersonde, I., Spector, O., Katzir, A. & Muller, G. (2000). *Proc. Soc. Photo. Opt. Instrum. Eng.* **4129**, 249–258.
Chan, Y.-H. M. & Boxer, S. G. (2007). *Curr. Opin. Chem. Biol.* **11**, 581–587.
Doshi, D. A., Dattelbaum, A. M., Watkins, E. B., Brinker, C. J., Swanson, B. I., Shreve, A. P., Parikh, A. N. & Majewski, J. (2005). *Langmuir*, **21**, 2865–2870.
Gagner, J., Johnson, H., Watkins, E., Li, Q., Terrones, M. & Majewski, J. (2006). *Langmuir*, **22**, 10909–10911.
Gibbons, W. J., Karp, E. S., Cellar, N. A., Minto, R. E. & Lorigan, G. A. (2006). *Biophys. J.* **90**, 1249–1259.
Goksu, E. I., Vanegas, J. M., Blanchette, C. D., Lin, W.-C. & Longo, M. L. (2009). *Biochim. Biophys. Acta*, **1788**, 254–266.
Hanzal-Bayer, M. F. & Hancock, J. F. (2007). *FEBS Lett.* **581**, 2098–2104.
Harroun, T. A., Kucerka, N., Nieh, M. P. & Katsaras, J. (2009). *Soft Matter*, **5**, 2694–2703.
Hsiai, T. & Berliner, J. A. (2007). *Curr. Drug Targets*, **8**, 1222–1229.
Jablin, M. S., Flasiński, M., Dubey, M., Ratnaweera, D. R., Broniatowski, M., Dynarowicz-Łątka, P. & Majewski, J. (2010). *Biophys. J.* **99**, 1475–1481.
Markesbery, W. R. & Carney, J. M. (1999). *Brain Pathol.* **9**, 133–146.
Martinet, W. & Kockx, M. M. (2001). *Curr. Opin. Lipidol.* **12**, 535–541.
Matsuzaki, K., Murase, O., Sugishita, K., Yoneyama, S., Akada, K., Ueha, M., Nakamura, A. & Kobayashi, S. (2000). *Biochim. Biophys. Acta*, **1467**, 219–226.
McGillivray, D. J., Valincius, G., Vanderah, D. J., Febo-Ayala, W., Woodward, J. T., Heinrich, F., Kasianowicz, J. J. & Losche, M. (2007). *Biointerphases*, **2**, 21–33.
McIntosh, T. J., Vidal, A. & Simon, S. A. (2003). *Biophys. J.* **85**, 1656–1666.
Megli, F. A. & Russo, L. (2008). *Biochim. Biophys. Acta*, **1778**, 143–152.
Monzel, C., Fenz, S. F., Merkel, R. & Sengupta, K. (2009). *Chemphyschem*, **10**, 2828–2838.
Mozsolits, H. & Aguilar, M. I. (2002). *Biopolymers*, **66**, 3–18.
Nelson, A. (2006). *J. Appl. Cryst.* **39**, 273–276.
Nevot, L. & Croce, P. (1980). *Rev. Phys. Appl.* **15**, 761–779.
Parratt, L. G. (1954). *Phys. Rev.* **95**, 359–369.
Parthasarathy, R. & Groves, J. T. (2007). *Soft Matter*, **3**, 24–33.
Pedersen, J. S. & Hamley, I. W. (1994*a*). *J. Appl. Cryst.* **27**, 36–49.
Pedersen, J. S. & Hamley, I. W. (1994*b*). *Physica B*, **198**, 16–23.
Radhakrishnan, A. & McConnell, H. M. (1999). *Biophys. J.* **77**, 1507–1517.
Sackmann, E. (1996). *Science*, **271**, 43–48.
Schutz, G. J., Kada, G., Pastushenko, V. P. & Schindler, H. (2000). *EMBO J.* **19**, 892–901.
Simons, K. & Ikonen, E. (1997). *Nature (London)*, **387**, 569–572.
Slotte, J. P. (1999). *Chem. Phys. Lipids*, **102**, 13–27.
Smith, H. L., Hickey, J., Jablin, M. S., Trujillo, A., Freyer, J. P. & Majewski, J. (2010). *Biophys. J.* **98**, 793–799.
Smith, H. L., Howland, M. C., Szmodis, A. W., Li, Q. J., Daemen, L. L., Parikh, A. N. & Majewski, J. (2009). *J. Am. Chem. Soc.* **131**, 3631–3638.
Smith, H. L., Jablin, M. S., Vidyasagar, A., Saiz, J., Watkins, E., Toomey, R., Hurd, A. J. & Majewski, J. (2009). *Phys. Rev. Lett.* **102**, 228102.
Stauffer, T. P. & Meyer, T. (1997). *J. Cell Biol.* **139**, 1447–1454.
Wang, W., Fu, Y. J., Zu, Y. G., Wu, N., Reichling, J. & Efferth, T. (2009). *Arch. Virol.* **154**, 595–600.